ANALIZA COMPARATIVĂ A TRANSFERULUI DE CĂLDURĂ AL UNUI MATERIAL COMPOZIT AVANSAT DE IZOLAȚIE PENTRU CLĂDIRI PRIN UTILIZAREA PROGRAMELOR DE CALCUL COMSOL MULTIPHYSICS® ȘI MATLAB®
COMPARATIVE ANALYSIS OF HEAT TRANSFER FOR AN ADVANCED COMPOSITE MATERIAL USED AS INSULATION IN THE BUILDING FIELD BY MEANS OF COMSOL MULTIPHYSICS® AND MATLAB® COMPUTER PROGRAMS

S. PERILLI[1], M. REGI[2], S. SFARRA[1]*, I. NARDI[1]

[1]*Department of Industrial and Information Engineering and Economics, University of L'Aquila, Piazzale E. Pontieri no.1, I-67100, Monteluco di Roio – L'Aquila (AQ), Italy*

[2] *Department of Physical and Chemical Sciences, University of L'Aquila, Via Vetoio (Coppito 1), I-67100, Coppito – L'Aquila (AQ), Italy*

The aim of this work is the study of the thermal flux through a multilayer insulation specimen, whose final panels could be designed for the green building field. The specimen was fabricated using an expanded styrofoam base, the mortar and milk cements, a fiberglass, and hemp fibers chopped and scattered into a surface smoothing. The dimensions of the specimen are 230 x 75 x 30.2 [mm]. The need to analyze a reduced surface in the development of a 3D visualization follows a computational aspect, i.e., to limit the number of degrees of freedom to be solved. Specifically, the research is focused on a comparative analysis among numerical simulations through the data processing by means of Matlab® - using the finite difference method (FDM) in the 1D domain -, and Comsol Multiphysics® - using the finite element method (FEM), both in 2D and 3D domains -. In addition, an experimental analysis centred on the detecting of the sub-superficial fiberglass by means of infrared thermography (IRT) technique is carried out. A specific Matlab® script was also implemented.

Finally, can be observed that Comsol Multiphysics® not only allows a visualization of the flow, as it is done in Matlab®, but also of the entire specimen geometry with the possibility of realizing a video of the thermal transient during the heating and cooling phases.

1. Introduction

This work is focused on the analysis of an insulating specimen, depicted in Figure 1 and described, in its components, in Table 1. The main aim of this work is the comparison of the simulations performed with the software Comsol Multiphysics® computer program [1] and a Matlab® code [2].

The approach deals with the stationary and transient behavior for both the simulations, varying the thermal load from constant to oscillating.

The optimum heat flux to be provided by using two halogen lamps has been calculated thanks to an *ad hoc* Matlab® script. The latter takes into account both the relative intensity and spectral distributions of the Siccatherm® lamps, and the corrective coefficient linked to the degradation factors inherent to the lamps, such as the aging of the lightbulb and the loss or gain of irradiance during the time of exposure. However, two thermographic scenery are reported and analyzed through an advanced processing technique explained in detail into section 4. The difference in the results confirms the experimental approach.

Although the utilization of the hemp fibers that constitute the external layer of the material under inspection, are not a news in the green building [3–5] field, the combined use of it, together with glass fibers (fulfilling to mechanical stresses such as an earthquake), can be considered as a technical innovation in the civil engineering field.

It will be explained how, although the adhesion between subsequent layers is usually not perfect, *i.e.*, porosity limits the ideal contact, the use of a simplified analysis during the simulation of the heat flux that reduces the contribution of convection and radiation phenomena, could be

---
* Autor corespondent/*Corresponding author*,
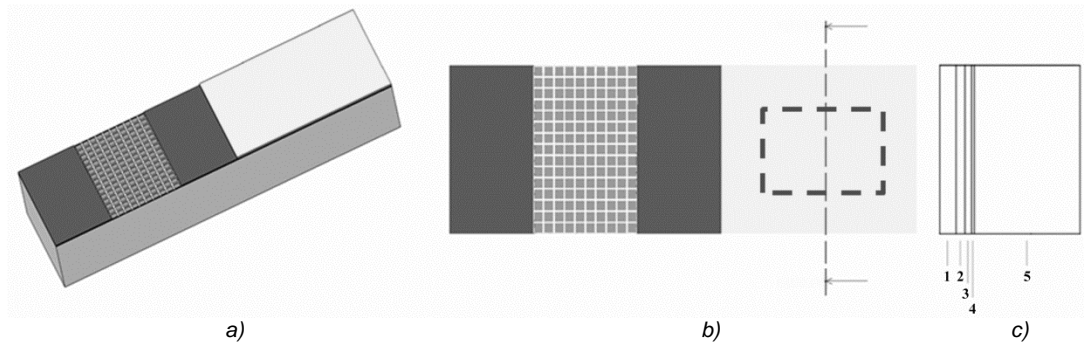E-mail: stefano.sfarra@univaq.it

Fig. 1 - The specimen: *a)* 3D view; *b)* front of view; *c)* cross-section in which the layers are numbered. The dotted rectangle is referred to the area into which the 3D simulations have been performed. Fig. *c)* has been reported on the right side of the top view of the specimen (instead of on the left side) for simplicity reasons.

Table 1

Technical characteristics of the specimen. The last column represents the porosity in term of % of the Volume

N.	Material	Thickness $[m]$	Conductivity(k) $\left[\frac{W}{m \cdot K}\right]$	Density(ρ) $\left[\frac{kg}{m^3}\right]$	Specific Heat(c_p) $\left[\frac{J}{kg \cdot K}\right]$	Emissivity (ε)	p % Vol.
1	Scattered Hemp Fibers	0.0010	0.038	25	1700.00	0.90	0.120
2	Cement Mortar	0.0005	1.73	900	0.21	0.54	0.220
3	Fiberglass	0.0002	0.035	21	1030.00	0.75	0.440
4	Cement Milk	0.0001	1.40	1540	0.87	0.92	0.147
5	Expanded Styrofoam	0.0286	0.03	30	1450.00	0.60	0.497

considered as a good compromise in order to reduce the computational process.

2. Technical characteristics of the hemp fibers and main information regarding the technological process

Hemp fibers for insulating and/or structural applications is derived from less fine parts of textile hemp. This material has breathability and good thermo-acoustic properties.

For the production, soda or boron salt are used; the product used for insulating purposes consists in a series of tiny compacted elements, while for structural purposes, it consists in continuous fibers.

Hemp fibers are recyclable and bio-compatible; the high Young-modulus (respect to a generic natural fiber), the low thermal and electric conductivity, along with the electromagnetic transparency let different applications and uses.

These fibers can be matched with polymeric or cement matrixes, thus are also used as structural reinforcement in the building sector, also because of the reduced cost if compared to glass fibers.

The main weak point of this material is its hygroscopic capacity, that forbid its employment directly in contact with liquids or in humid zones.

In order to minimize the negativity, in the present case the fibers of the external layer were coated with a binder, which performs a protective action, also limiting its hygroscopicity.

The latter effect was also limited in the layer by working under the ultrafine grinding conditions.

Ultrafine grinding is an energy-intensive stage in the overall of the process, which provides materials in the proper size range for the required properties of final product. The optimization of the product obtained has been conducted by using a mill working at high energy (velocity = 2000 min^{-1}), bearing in mind that a few mm[2] have been required in order to finalize the layer. The combination of the impact (between the spheres and the aggregates), the friction and the circular movement of the ceramic jar having an oval shape, generated a compound that summarized the best characteristics coming from the mixer-mill, the disc mill and the planetary mill with spheres. The final compound similar to an homogeneous flour, was applied through a modified spray gun.

In the following, both the heat transfer principles and the related modeling approaches are described [6].

3. Heat Transfer Modeling

3.1. Basics of physics

The diffusion equation, without inner energy production rate, and neglecting convection and radiation flux energy, in the 3D domain is expressed by the Laplace law:

$$\frac{\partial T}{\partial t} = \alpha \nabla^2 T \qquad (1)$$

For 1D domain, that corresponds to an infinite slab configuration, the Equation 1 is reduced to $\frac{\partial T}{\partial t} = \alpha \frac{\partial^2 T}{\partial x^2}$, where α is the thermal

diffusivity, defined as $= \frac{k}{c_p \rho}$.

Given a specimen made of N different layers, it is possible to characterize it by providing geometric and mass characteristics, along with thermo-physical properties, *i.e.*, specific heat at constant pressure c_p, density ρ and material's conductivity k of each layer [7].

3.1.1. Matlab® approach

In order to proceed with a Matlab® analysis, it is necessary to convert a Partial Differential Equation (PDE) to an Ordinary Differential Equation (ODE) through a finite difference method. This transition requires the implementation of a dedicated calculation code, that operates the discretization of the system beginning from the thickness that is now expressed as:

$$S = \sum_{i=1}^{N} S_i \qquad (2)$$

where, S_i indicate the thickness of the ith layer. In order to obtain the optimal discretization for the method integration, the adopted criteria for choosing guarantees that, in any generic step of the analysis, there is the same material. This ensures that, in one or more border zones, there is coincidence of the integration nodes for the solution.

For this aim, the total thickness is divided in a reasonable number of equal parts, obtaining the following:

$$\Delta x = \frac{S}{M} \qquad (3)$$

where, M is chosen imposing that the minor layer is subdivided into sufficient number of sub-meshes. Therefore, at the jth depth, it is:

$$x_j = j\Delta x \qquad (4)$$

In order to operate the discretization of the ∇ operator for a one-dimensional system, the authors introduce the finite difference of the first and second order, by obtaining [8]:

$$\frac{\partial T_j}{\partial x} \cong \frac{T_{j+1} - T_j}{\Delta x}, \qquad (5)$$

and, for the second derivative, by introducing:

$$\frac{\partial T_{j+1}}{\partial x} \cong \frac{T_{j+2} - T_{j+1}}{\Delta x}. \qquad (6)$$

Therefore, it is obtained:

$$\frac{\partial^2 T_j}{\partial x^2} \cong \frac{\frac{\partial T_{j+1}}{\partial x} - \frac{\partial T_j}{\partial x}}{\Delta x} = \frac{T_{j+2} - 2T_{j+1} + T_j}{\Delta x^2} \qquad (7)$$

that has to be centered in *j+1*. At this point, the equation becomes:

$$\frac{\partial T_j}{\partial t} = \alpha_j \frac{T_{j+2} - 2T_{j+1} + T_j}{\Delta x^2} \qquad (8)$$

that is resolvable once initial and boundary conditions are imposed. Particular attention must

be paid in the contact of different materials. Hypothesizing a perfect interaction, the jth and $j+1^{th}$ discretization that belongs to the ith interface is governed by the following equation:

$$\alpha_j \left(\frac{\partial T_j}{\partial x} \right) = \alpha_{j+1} \left(\frac{\partial T_{j+1}}{\partial x} \right) \qquad (9)$$

By introducing Eq. (9) in Eq. (8), the flow continuity through the layers is guaranteed thanks to Eq. 10.

$$\frac{\partial T_j}{\partial t} = \frac{1}{\Delta x^2} \left[\alpha_{j+1} T_{j+2} - (\alpha_j + \alpha_{j+1}) T_{j+1} + \alpha_j T_j \right] \qquad (10)$$

These relations can be implemented in a recursive form by the function f_{name} in Matlab® environment; therefore, it is possible to solve the heat diffusion problem using an appropriate Ordinary Differential Equations (ODE) solver. In the present analysis, the *ode15s* was used; this, because it solves both the stiff differential equations and the Differential Algebraic Equation (DAE)$_s$ variable order method.

3.1.2. Comsol Multiphysics® approach

In the Comsol® analysis, a finite element method was used by accessing into multi-physics section with the **out-of-plane** function, and through Eq. 11.

$$d_z \rho C_p \frac{\partial T}{\partial t} + \nabla \cdot (-d_z k \nabla T)$$
$$= d_z Q + d_z q_s T + h_u (T_{ext,u} - T)$$
$$+ \varepsilon_u \sigma (T_{amb,u}^4 - T^4)$$

$$(11)$$

where, d_z is the thickness out-of -plane, q_s is the coefficient of production/absorption, h_u is the convective coefficient, ε_u is the superficial emissivity, $T_{ext,u}$ is the outer surface temperature, and $T_{amb,u}$ is the outdoor temperature.

Comparing the previously equation with the Eq. 1, it is possible to obtain:

$$d_z \rho C_p \frac{\partial T}{\partial t} + \nabla \cdot (-d_z k \nabla T) = 0 \qquad (12)$$

In this work, a triangular mesh has been used, by obtaining the mesh shown in Figure 2.

In Figure 2a, the mesh grid is reported, while in Figure 2b there is an enlargement that highlights the coherence of the nodes at the interfaces between different materials. This result guarantees the continuity of the topological analysis and, in the same time, it confirms the proper choosing of the boundary equation, similarly to Matlab® approach [9].
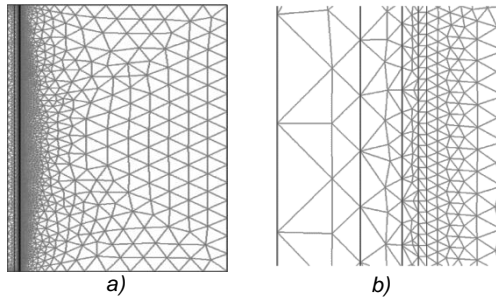
Fig. 2 - *a)* 2D complete mesh, and *b)* 2D detail of the mesh.

The thermal stress provided, and described in the following, underlies the heating phase that, together with the natural cooling phase, it has been analyzed through the infrared thermography method, using the Principal Component Thermography (PCT) technique illustrated in the following.

4. Principal Component Thermography (PCT) technique

This technique allows the decomposition to single values, since it expresses the tensor of thermograms as a matrix of the values of the thermographic sequence $\boldsymbol{A}_{(\underline{M}\times\underline{z})}$, where the rows of $\boldsymbol{A}$ (*i.e.*, $\underline{M} = \underline{n}_x \times \underline{n}_y$) contain the information in pixel of each thermogram, and the columns $\underline{z}$ the number of thermograms.

$$\boldsymbol{A}_{(\underline{M}\times\underline{z})} = \boldsymbol{U}_{(\underline{M}\times\underline{z})} \cdot \underline{S}_{(\underline{z}\times\underline{z})} \cdot \underline{V}^T_{(\underline{z}\times\underline{z})} \qquad (13)$$

Particular interest assumes the Empirical Orthogonal Functions (EOF), namely the columns of the tensor $\boldsymbol{U}$ that, if arranged as the sequence of thermograms, it generates the images in which the sub-superficial discontinuities are detectable [10].

5. Experimental setup, results and discussion

From the analysis previously explained, it is evident a purely modeling construction in the Matlab® approach, where the choice of the integration interval is strictly dependent on the specific model; the elaboration set up allows the analysis of models of indefinite dimension in the plane, using an appropriate spatial interval *Δx* out-of-plane, according to the specific needing. Simultaneously, Figure 3 obtained by Matlab® shows a trend analogous to Figure 5 coming from Comsol Multiphysics® computer program, and for both methods, the steady state condition is achieved after *t* = 500 [s]. Similar conclusions are attributable to the transient case study.

For what concerns Comsol Multiphysics®, the model is built in two dimensions (out-of-plane), assigning the couples of interfaces, that look like lines, and by obtaining the three-dimensionality tuning on the mesh. This was possible, since the

size of the plane was constant for each layer of the material. The choice based on the realization of the three-dimensionality using the mesh, it allows an easier (computationally) analysis, by avoiding the study of the out-of-plane boundary effects.

As anticipated above, numerical simulations have been performed for the steady-state and transient conditions. In the first case scenario, the contribution of the convection and radiation phenomena, it was before neglected and after considered in a second time. The results show how, in the present case, the simplified analysis is in good agreement with the complete mathematical model, at least for the main points of interest linked to an insulation panel.

The validation of the heat flux distributed on the specimen surface has been performed by using PCT technique.

5.1. Steady State condition

For the steady state scenario, Eq. 1 becomes the Laplace law with a well-known temperature profile for a multilayer slab system. This equation can be solved using the previously assumptions. In this experiment, the authors assume that the temperature imposed to the specimen at the initial time $t_0 = 0$ is uniform and equal to 10 [°C] (283.15 [K]). The temperature of the rooms that face surface 1 and surface 5 in Figure 1 are supposed equal to 15 [°C] (288.15 [K]) and 10 [°C] (283.15 [K]), respectively.

5.1.1 Matlab® approach

The spatial discretization *Δx* was chosen equal to 1/5 of the minimum thickness expressed in Table 1, namely $\Delta x = 2 \cdot 10^{-5}$ [m]. In this configuration, the following results (Fig. 3) have been obtained.

Therefore, the model is not affected from boundary effects; in Figure 3a is shown the temporal variation of the temperature field through the thickness of the model, from the initial to the steady state condition. Besides, in Figure 3b is shown, along the thickness, the trend of temperature; the latter is indicated in the legend, while the different levels represent the time step, up to the steady state condition.

However, for a one-dimensional system, the differential equation that establishes the temperature variations in relation to the position *x* and the time *t*, and that takes into account the radiation energetic transfer phenomena, *i.e.*, convective and diffusive, is:

$$\rho c_p \frac{\partial T}{\partial t} = \nabla(k\nabla T) + \varepsilon\sigma(T_{ext}^4 - T^4) - h(T_{ext} - T) \quad (14)$$

In Eq. (14), T_{ext} represents the outside temperature in contact with the walls, T is the generic temperature in a specific point of the system, $\sigma = 5.67 \cdot 10^{-8}$ W/(m²K⁴) is the Stefan-Boltzmann constant, and h is the aeriform
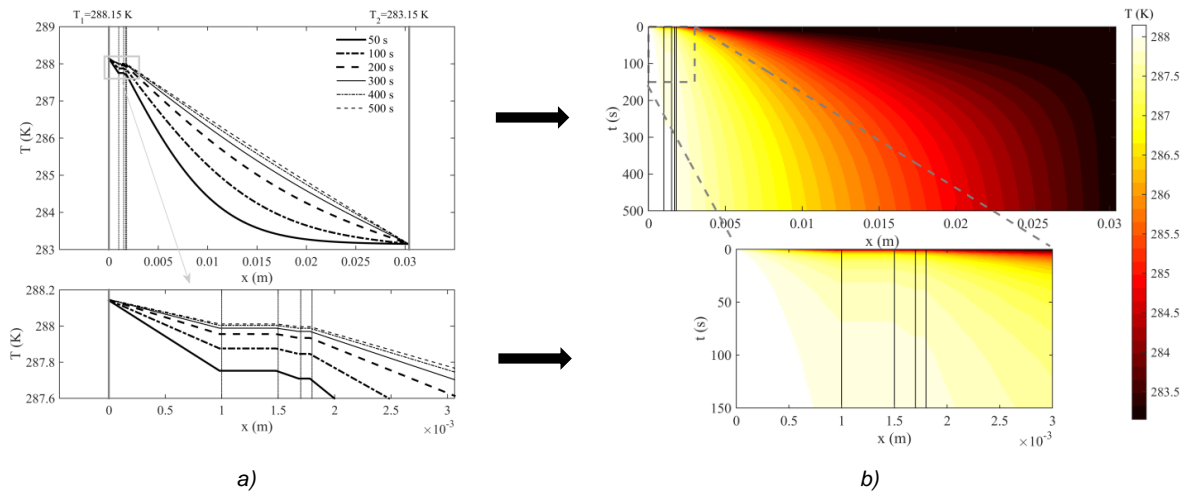
Fig. 3 - Trend of temperature during the transient state. The black and white identify: *a)* the timing, or *b)* the temperature. *See the color figure on the online journal.*

convection coefficient equal to 6 $\left[\frac{W}{m^2 \cdot K}\right]$. In this problem, the diffusion of the matter has been neglected (*i.e.*, the advection). The problem can be more relevant in case the porosity of the material is taken into account; indeed, it is linked to a reduction of the thermal conductivity of the entire system.

From now on, a multilayer system is considered. As in the case of the purely diffusive system, the heat flux in the interface regions must be preserved. The latter condition has been imposed. In the entire system, the porosity seen as a reduction factor of heat transfer has been considered. In particular, the authors considered the porosity in correspondence of each substrate, as well as in the separation regions between layers of different materials, as described in the follow.

In each substrate of the same material having a thermal diffusivity equal to $\alpha = k/\rho c_p$, the heat diffusion transfer has been solely considered. If the porosity doesn't acts, the diffusion process would occur through the infinitesimal volume $dV = \Sigma dx$ containing uniformly material of the same type. In the latter, Σ represents the unit area, while dx is the infinitesimal thickness in the substrate.

Owing to porosity, the volume that contains the available matter for the diffusive heat exchange is a fraction of the simplified model (*i.e.*, the model schematized in the absence of porosity). In particular, $dV_{real} = (1-p)dV$. Therefore, the differential equation within each *h*-th substrate, is equal to:

$$\frac{\partial T}{\partial t}\bigg|_h = (1 - p_h)\alpha_h \frac{\partial^2 T}{\partial x^2}\bigg|_h \tag{15}$$

As part of the *Finite Difference Method*, by following the *Forward Difference* schematization,

Eq. (15) was developed as follows:

$$\frac{\partial T_i}{\partial t}\bigg|_h = (1 - p_h)\frac{\alpha_h}{\Delta x^2}(T_i - 2T_{i+1} + T_{i+2})_h \tag{16}$$

Taking into account that two materials of different type was putted in contact, and that this contact is not perfect in term of adhesion, therefore, in the intermediate region between the materials, the presence of the substrates are characterized by different porosities and by different temperature. In these regions, the continuity of the heat flow is guaranteed; the latter, similarly to the simplified case, *i.e.*, based on a purely diffusive process, as well as perfect in term of contact. However, the porosity constitutes a complication, at least formally, during the expression of the equation that establishes the conservation of the heat flux between two different materials.

Simply, the authors hypothesized that the heat flux Q_j that comes from a *j*-th layer (*i.e.*, it is linked to the right side of the *h*-th layer that "see" the left side of the next *h+1*-th layer) is equal to the sum $Q_j = Q_j^\alpha + Q_j^R$ of the fluxes by diffusion Q_j^α and by radiation Q_j^R, respectively.

For the same unit of surface Σ, a fraction of it not perfectly in contact between the substrates will be approximately proportional to a factor *p*. Consequently, the heat diffusion will be proportional to *1-p_h* and the radiation contribution to *p_h*.

In these regions was considered that the heat transfer takes place both by diffusion and by irradiation; therefore, the *Ordinary Differential Equation* (ODE) into the field of the *Forward Difference* schematization, it takes the following form:
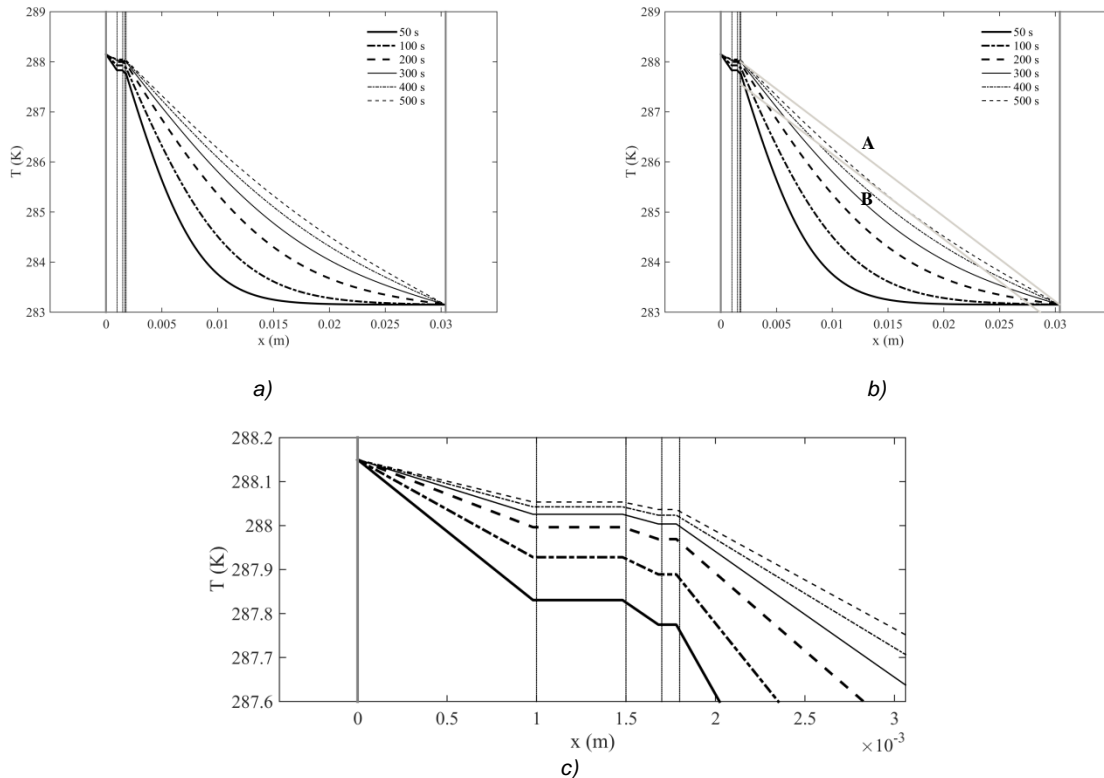
$$\frac{\partial T_j}{\partial t}\bigg|_h = \frac{1}{\Delta x^2}\left\{(1 - p_h)\alpha_h T_j - (1 - p_h)\alpha_h + \left[1 - p_{h+1}\alpha_{h+1}T_{j+1} + (1 - p_{h+1})\alpha_{h+1}T_{j+2}\right]\right\} + \frac{\epsilon_h \sigma}{(\rho c_p)_h} p_h\left(T_{j+1}^4 - T_j^4\right) \tag{17}$$

a)

b)

c)

Fig. 4 - Comparison at different time instants between the multilayer system: *a)* panel with porosity and boundary conditions to the left of the first layer based on convection and radiation phenomena, *b)* the same panel shown in *a)* with added the linear trend obtained into the layer 5 for non-porous conditions, and *c)* shows the details of the trend of temperature of the first layers starting from the top.

where, the first two terms on the right of Eq. (17) are related to the conductive process, while the last one is linked to the radiation process.

In the case of a multilayer manufactured by different materials listed in Tab. 1, the following results have been obtained. On the left of the layer 1 (Fig. 1), the temperature will gain equilibrium because the wall is strictly in contact with a fluid (air); this effect happened under conditions of radiation and convection, in which the temperature arrived at 288.15 K (*i.e.*, the initial temperature of the air) starting from T = 283.15 K (*i.e.*, the internal uniform temperature). Instead, on the right of the layer 5 (Fig. 1), the material exchanged energy by conduction and radiation with a T = 283.15 K, identical to the initial temperature, *i.e.*, permanent in the course of time.

In Figure 4, the temperature profiles at 500 s (by operating with 1000 temporal subdivisions) obtained by solving Eqs. (16) and (17) are shown. In particular, Figure 4a shows the case that includes the condition of porosity. In Figure 4b, the segment **A** indicates the trend during the steady state condition for a non-porous specimen, while the segment **B** represents the tangent to the curve of the steady state condition for a simulation representing the porous specimen. In this condition, the same slope denotes the position of the maximum ΔT obtained in the middle of the layer 5 (Fig. 1) for a value < 0.5 K. A similar procedure carried out on the radiative and

convective phenomena internal to the material is shown in subsection 5.1.2 linked to COMSOL Multiphysics® computer program.

For the sake of clarity and ease of reading to the readers, the trend of temperature of the first layers starting from the top of the specimen has been enlarged in Figure 4c.

In a separate analysis the authors tested the validity of the formulation proposed; in particular, they computed the temperature profiles at 500 s, assuming that the temperatures on the left of the layer 1 and on the right of the layer 5 (Fig. 1) were equal to the internal temperature. The relative % error of the computed temperature with respect to the predicted one was < 10^{-6}.

5.1.2. Comsol Multiphysics® approach

In this processing, it has been chosen the stationary solver named (**UMFPACK**), obtaining the following trends in Figure 5.

The trends shown both in Figure 5 and Figure 6 were obtained with transient solver, but the choice of the range (0, 10, 500 [s]) was made after a steady state analysis (previously illustrated in detail) that indicates the time of solving.

The three-dimensionality of the model is clear looking at Figure 6, where the different layers represent the temperature field at specific timing; it
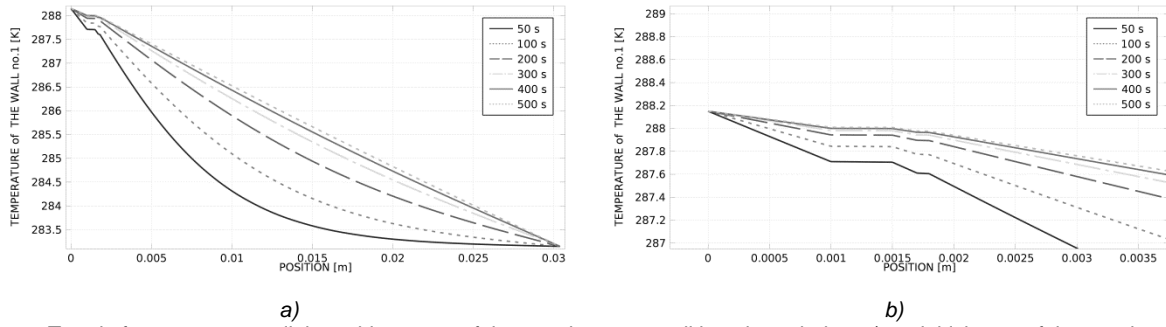
a)   *b)*

Fig. 5 **-** Trend of temperature until the achievement of the steady state condition, through the: *a)* total thickness of the specimen; *b)* magnification of the first part of the curves reported in Fig. 4a. The legend express the time in [s].

$$d_z \rho c_p \frac{\partial T}{\partial t} + d_z \rho c_p \mathbf{u} \cdot \nabla \mathrm{T} = \nabla \cdot \left(d_z k_{eff} \nabla \mathrm{T} \right) + d_z Q + Q_{oop} \tag{18}$$

$$Q_{oop} = \varepsilon_u \sigma \left(T_{amb,u}^4 - T^4 \right) + \varepsilon_u \sigma \left(T_{amb,d}^4 - T^4 \right) \tag{19}$$
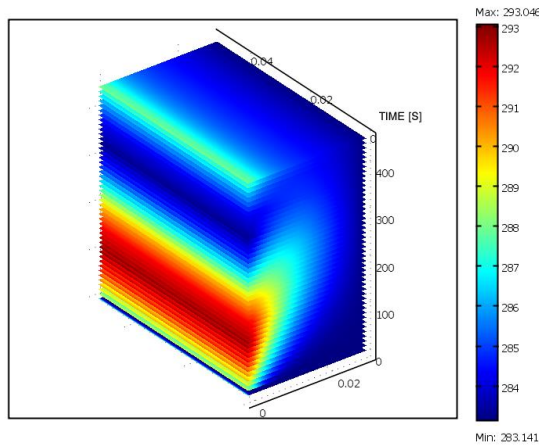

Fig. 6 **-** Temperature variation [K] until steady state. *See the color figure on the online journal.*

also shows the field related to the evolution in the plane. In particular, Figure 6 is linked to the dotted rectangle marked in Figure 1b.

In order to validate the results obtained through the previous analysis, that is more simple from the computational point-of-view (but also rigorous), in the following the result obtained after a complete analysis is reported. Bearing in mind this point, the transient's case follows the same rules, *i.e.*, the approximation made by the authors for the steady state scenario can be considered reasonable.

The complete analysis is linked to the version 5.1 of the Comsol Multiphysics® computer program through the **out-of-plane-radiation** function that follows the set of equations 18 – 19, where, the explanation of the greatest part of the terms is shown right after Eq. (11), while the missing terms represent: Q_{oop} is the radiation contribution, while $T_{amb,u}^4$ and $T_{amb,d}^4$ are the ambient temperatures with respect to the upside and downside parts of the specimen, respectively. In Tab. 1, the emissivity values adopted [11–13] are indicated, along with the porosity values [14–17].

The term $\left(d_z k_{eff} \nabla \mathrm{T} \right)$ has $[-\mathbf{n} \cdot \left(d_z k_{eff} \nabla \mathrm{T} \right) = d_z \mathrm{h} \cdot \left(T_{ext} - T \right)]$ as condition to the wall. The latter highlights the convection phenomena, for which, it was considered a natural convection. In the case used herein, *i.e.*, **surface-to-surface radiation**, it was set a thickness equal to 0.0304 [m], by considering entirely the specimen under inspection. From these considerations, the following trends (Fig. 7) were obtained.

As shown in Figure 7a, the trend of temperature differs from the simplified analysis (Fig. 5) only for the equilibrium condition that does not present a rectilinear slope. In Figure 7b, through the straight line **A**, the trend obtained by the simplified analysis is reproduced. Instead, through the straight line **B**, that is parallel to the previous one, the point of greatest discrepancy of the temperature value indicated by **C** is detected thanks to the tangent of the trend of the equilibrium. In particular, a magnification of the trend of temperature of the first layers is reported in Figure 7c in order to emphasize their contribution in the relaxing phase of the thermal wave. It is possible to notice that the maximum temperature difference is present at 0.013 [m] in depth, *i.e.*, at approximately half of the Expanded Styrofoam (layer 5 in Fig. 1), for a ΔT <1 [K]. Because both the extreme values and the general trend of the temperatures are confirmed, it is possible to say that the simplified analysis, applied for the specific case, can be used by helping the computational processes. This corollary corroborates and validates what has been already shown in subsection 5.1.1, since the graphical determination of the tangent line to the curve was the same of the simulation performed by the Matlab® computer program. The small difference of about 0.5 [K] among the computer programs can be possibly attributed to a variability of the building of the meshes that in Comsol Multiphysics® is automatized with a refined shape, while in Matlab® is directly assigned by Eq. (3).
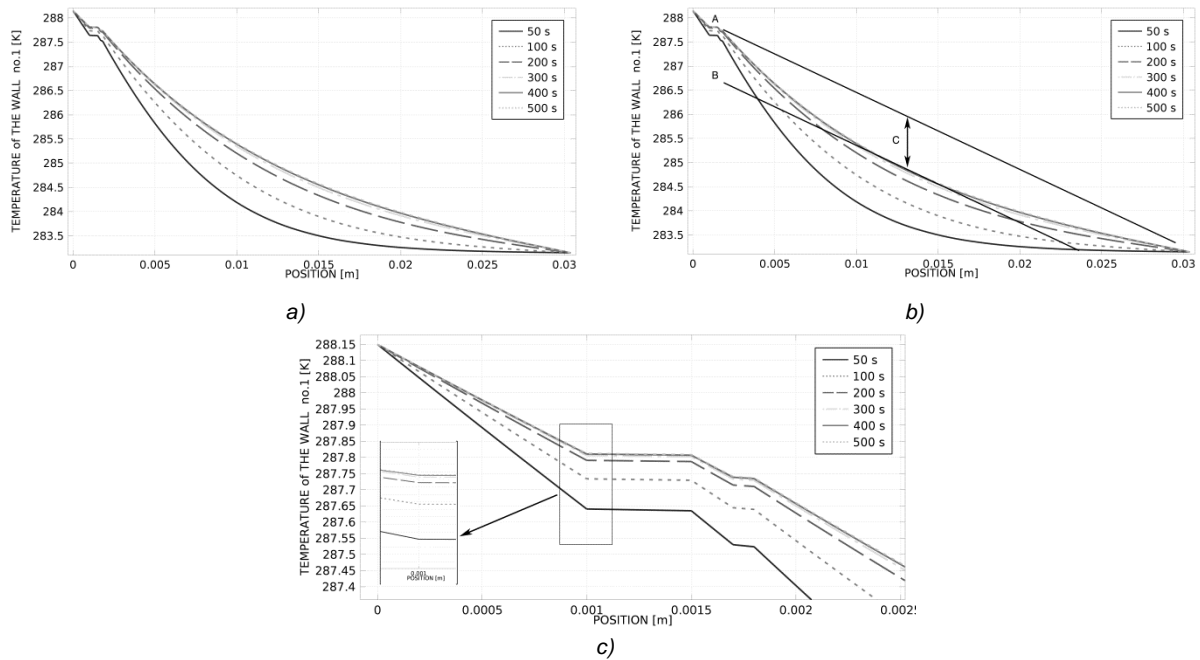
a)

b)

c)

Fig. 7 - Trend of temperature until the achievement of the steady state condition, through the: *a)* complete analysis, and *b)* complete analysis with a comparison with respect to the simplified analysis. Fig. *c)* shows the details of the trend of temperature of the upper layers, *i.e.*, the presence of 6 curves, similarly to Fig. 4c. The legend express the time in [s].
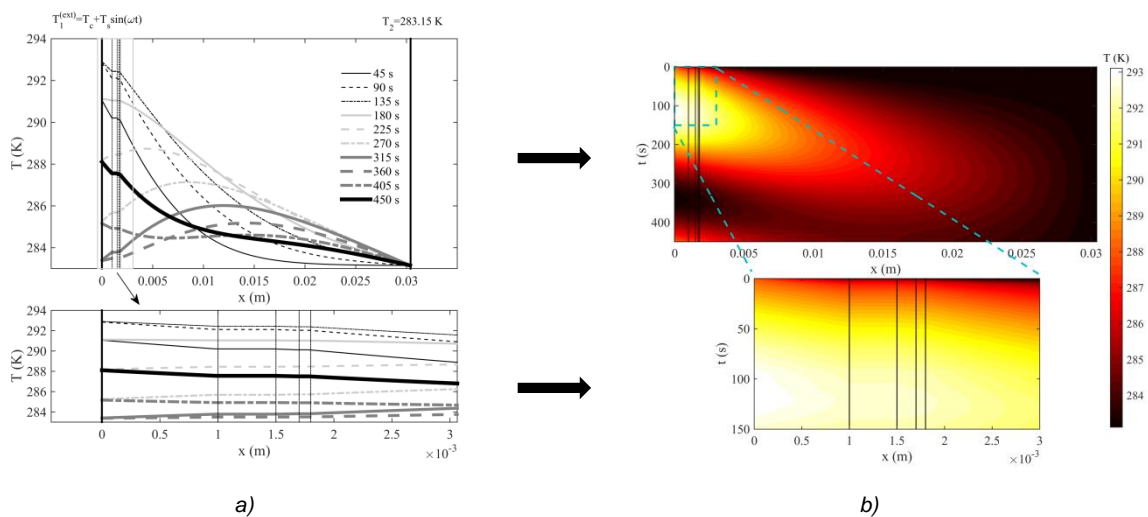

a)

b)

Fig. 8 - Trend of temperature. The black and white identify: *a)* the timing, or *b)* the temperature. *See the color figure on the online journal.*

5.2. Transient state condition

For the transient state, given the initial uniform temperature equal to 15 [°C] (288.15 [K]), it has been imposed that the temperature of the first layer varies with the law $T_1^{(ext)} = T_c + T_s.sin(\omega t)$ at the generic time $t > t_0$, being $T_c = 10[°C]$, and $T_s = 5[°C]$ and $P_1 = 2\pi/\omega = 450$ [s]. For the layer number 5 (Fig. 1), it has been imposed a constant and uniform temperature $T_5^{(ext)} = 10$ [°C]. On the basis of the experience gained during the treatment of the steady state condition, in this case the authors solely considered the diffusive phenomenon (*i.e.*, without the addition of the convection and radiation contributions), by excluding the influence of the porosity inside the specimen.

5.2.1. Matlab® approach

Using the discretization discussed in subsection 3.1.1., and imposing the oscillating boundary conditions on the surface number 5 (Fig. 1), the following trends have been obtained (Fig. 8). Analogous considerations can be made for the oscillating case; Figure 8 shows the graphs centered at $T = 288$ [K].

5.2.2. Comsol Multiphysics® approach

Setting an oscillating boundary condition, and using the (**UMFPACK**) function, the following trends have been obtained (Fig. 9).
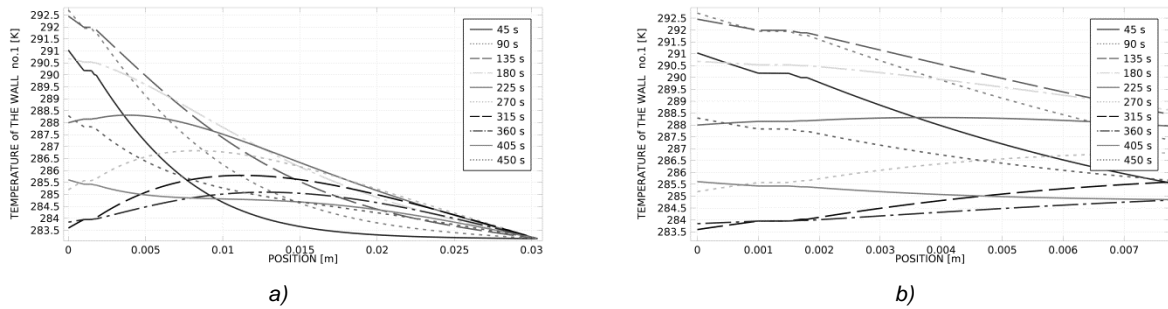
S. Perilli, M. Regi, S. Sfarra, I. Nardi / Analiza comparativă a transferului de căldură al unui material compozit avansat
de izolație pentru clădiri prin utilizarea programelor de calcul Comsol Multiphysics® și Matlab®
193

a)   *b)*

Fig. 9 **-** Trend of temperature with oscillating boundary condition, through: *a)* the total thickness of the specimen; *b)* magnification of the first part of the curves reported in Fig. 9a. The legend express the time in [s].

Also in this case, the three-dimensionality of the model is clear looking at Figure 10, where the different layers represent the temperature field at specific timing; it also shows the field related to the evolution in the plane. In particular, Figure 10 is linked to the dotted rectangle marked in Figure 1b.

Fig. 10 **-** Temperature variation [K] with oscillating boundary condition. The layers represent the temperature field that is shown in the various temporal instants reported in the vertical axis. *See the color figure on the online journal.*

Analogous considerations inherent to the trend of temperature can be made for the oscillating case (Fig. 9 and Fig. 10); therefore, in Figure 9a, the graph goes from the maximum to the minimum value, by seeing it from the left to the right side.
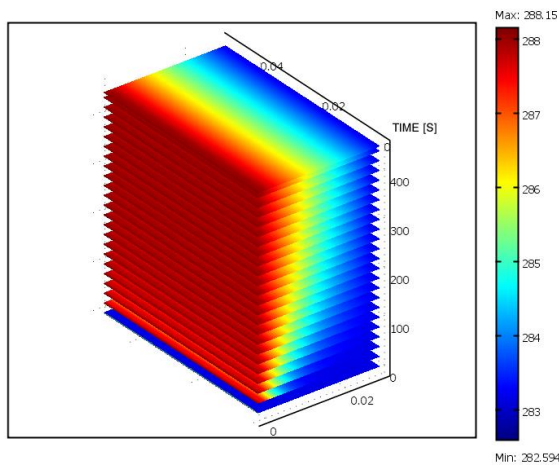
5.3. Active InfraRed Thermography analysis

The experimental set up related to this method is based on Figure 11. Into the latter, the most important technical data are shown.

Two OSRAM Siccatherm® lamps, each of 250 [W], have been used during the experiment [18]. The thermographic campaign consisted in two sessions: in the first one, the heating phase lasted 60[s], and the cooling phase 180[s]; in the second one, they lasted 120[s] and 380[s], respectively. The first session had 240 thermograms, while the second had 500 thermograms. In both cases, the frame rate was set at 1 thermogram per second.

As said in section 1, using a script written *ad hoc* in Matlab® environment, the view factors illustrated in Figure 12 have been calculated and plotted [19].
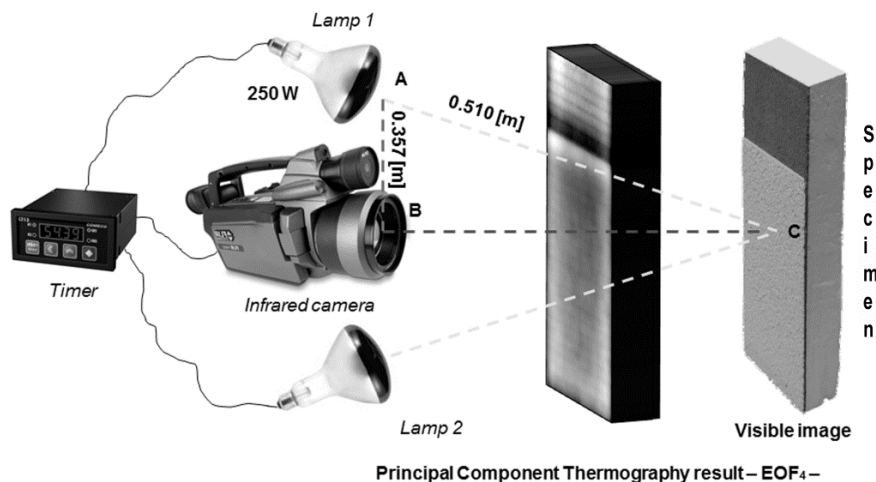

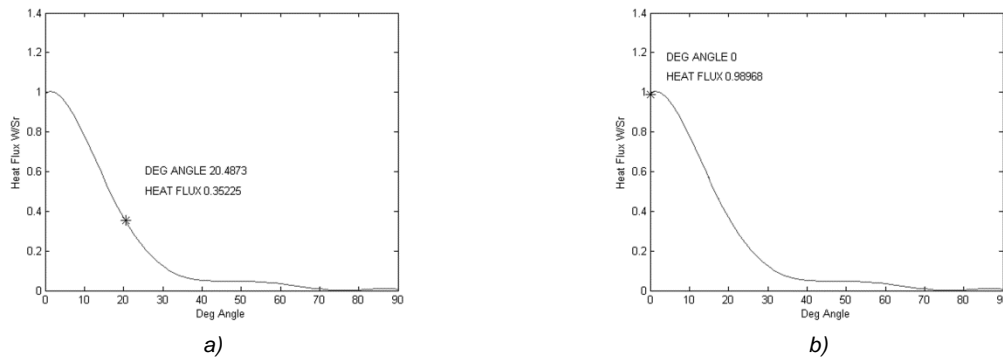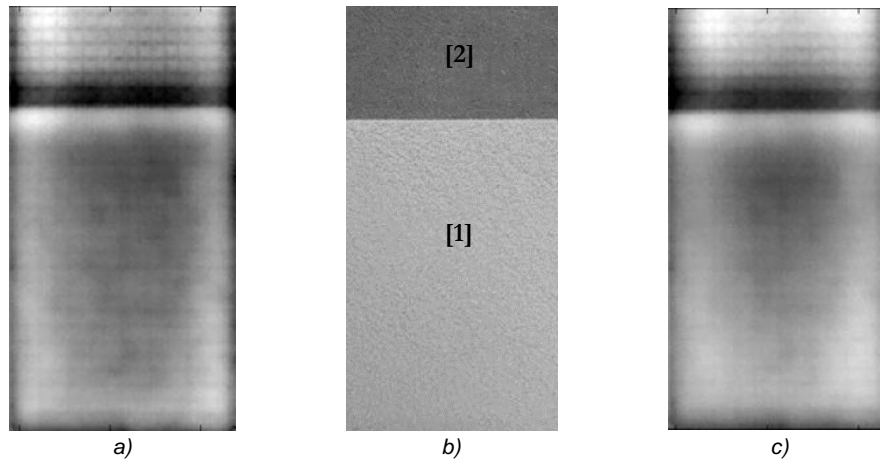**Fig. 11 -** IRT experimental setup.

a)

b)

Fig. 12 - View factors: *a)* horizontal, and *b)* vertical.

a)   *b)*   *c)*

Fig. 13 - *a)* PCT EOF$_4$ after 60 [s] of heating, *b)* visible image, and *c)* PCT EOF$_4$ after 120 [s] of heating.

The graphs refer only to lamp 1, since the results obtained from lamp 2 won't vary. Indeed, it is arranged conversely. The total flux measured was equal to 9902 [W/m^2] that corresponds to 111.39 [W] administered on the front face on the specimen. It is evident that the experiment is linked to the steady state condition.

In Figure 13, both the visible image and the PCT EOF$_4$ results - by processing together the heating and the cooling phase - are shown; it can be seen how the presence of the reinforcement net in glass fiber beneath the layer made by scattered hemp fibers **[1]** is much more evident in Figure 13a. Readers can refer to Figure 13b for comparison purposes. This is due to the temperature gradient; indeed, in the second experiment, the heating phase lasted more, so the heat gained a much deeper layer of the specimen. In particular, in Figure 13c the sub-superficial features are less contrasted.

The same happens by seeing the surface **[2]**. During the PCT technique, thermograms have been acquired using an IR camera made by FLIR and working into the long wave (LW) infrared spectrum (9.5-13 µm); subsequently, raw thermograms have been analyzed thanks to a specific computer program [20]. The results provided by this technique allow both to optimize the contrast and to minimize uneven heating.

Taking into account the depth of the reinforcement net in glass fiber, its detection inside the zones **[1]** and **[2]** reflects the rules introduced by [21] and [22]. Indeed, the observation time *t* is a function (in a first approximation) of the square of the depth *z* and the loss of contrast *c* is proportional to the cube of the depth:

$$t \approx \frac{z^2}{\alpha} \ and \ c \approx \frac{1}{z^3} \tag{20}$$

where, α is the thermal diffusivity of the material. These two relations show two limitations of pulsed thermography, *i.e.,* observable defects will generally be shallow and the contrasts weak [23]. An empirical rule of thumb says that the radius of the smallest detectable defect should be at least one to two times larger than its depth under the surface [24].

The use of a square pulse combined with a PCT processing like in the present case maximizes the solving of these limitations.

6. Conclusions

The aim of the work was the comparison of Matlab® and Comsol Multiphysics® computer programs when applied together in the heat transfer modeling of a complex case scenario like multilayer panels devoted to building field. In both Matlab® and Comsol® informatics languages, the multilayer system was easily implemented into their respectively codes, before solving the PDE

problem: the Matlab® language requires an appropriate code that can be adapted for a general multilayer case study, while Comsol® computer program requires an appropriate 3D realization of the multilayer system.

The results obtained were in agreement, and they were focused on the study of the entire thickness of the specimen under analysis. The results were also in agreement when the convection and radiation phenomena were taken into account during the explanation of the steady state scenario, since at the contact between different layers of material, where the manufacturing process cannot guarantee a perfect adhesion, the transfer phenomena can also occur by following these conditions. Because the ultrafine grinding was adopted during the fabrication of the specimen, at least for the layer 2., it is possible to assume that porosity was very limited at the respective interfaces and the modeling, putting in practice this condition, tended to minimize these fundamental contributions that, otherwise, cannot be neglected [25].

The possibility of the development of a 3D model, only for the mesh grid, highlights the opportunity to also consider the boundary effects (out-of-plane) by assuming an indefinite layer in the plane. Instead, using the PCT technique it is possible to identify the presence of the fiberglass net beneath the cement mortar. It is not possible to see this detail in the models, since, even for the Comsol Multiphysics® computer program, the fiberglass modeled – as warp and woof geometry – it has not been used. The latter, indeed, has been assimilated to a line, homogeneous and continuous in the 2D plane; it was also extended into the mesh, by providing a behavior like a continuous panel. As a future development of the work, a 3D model will be implemented directly from a solid, using the version 5.1 of Comsol Multiphysics®, that will let the introduction of a composite net, by ensuring in the same time the interface continuity between the fiberglass net and the materials adjacent to it [26]. In addition, the thermograms will be analyzed through the Wavelet Transform Thermography (WTT) technique that allows, using a coherence analysis, the minimization of the user's discretional contribution in the choice of the best result to be visualized at the end of the image processing [27].

REFERENCES

1. T. Behzad, M. Sain, Finite element modeling of polymer curing in natural fiber reinforced composites, Compos Sci Technol 2007, **67**, 1666.
2. L. G. Thygesen, P. Hoffmeyer, Image analysis for the quantification of dislocations in hemp fibres, Ind Crop Prod 2005, **21**, 173.
3. F. Pacheco-Torgal, S. Jalali, Cementitious building materials reinforced with vegetable fibres: a review, Constr Build Mater 2011, **25**, 575.
4. S. Elfordy, F. Lucas, F. Tancret, Y. Scudeller, L. Goudet, Mechanical and thermal properties of lime and hemp concrete ("hempcrete") manufactured by a projection process, Constr Build Mater 2008, **22**, 2116.
5. J. K. Panday, S. H. Ahn, C. S. Lee, A. K. Mohanty, M. Misra, Recent advances in the application of natural fiber based composites, Macromol Mater Eng 2010, **295**, 975.
6. S. Sfarra, C. Ibarra-Castanedo, C. Santulli, S. Sarasini, D. Ambrosini, D. Paoletti, X. Maldague, Eco-friendly laminates: from the indentation to non-destructive evaluation by optical and infrared monitoring techniques, Strain 2013, **49**, 175, DOI: 10.1111/str.12026.
7. D. Q. Kern, Process Heat Transfer, Mc Graw-Hill Book Company SPL, Singapore, 1965.
8. G. Monegato, Fondamenti di calcolo Numerico, Libreria Editrice Universitaria Levrotto&Bella, Turin, 1990.
9. B. Y. Xue, S. C. Wu, W. H. Zhang, G. R. Liu, A smoothed FEM (S-FEM) for heat transfer problems, Int J. Comput. Methods, 2013, **10**, 1.
10. N. Rajic, Principal component thermography for flaw contrast enhancement and flaw depth characterization in composite structure, Compos Struct, 2002, **58**, 521.
11. Fluke, *http://support.fluke.com/findsales/Download/Asset/3038318_6251_ENG_A_W.PDF,* accessed on December 01, 2015.
12. I.M. De Rosa, F. Marra, G. Pulci, C. Santulli , F. Sarasini, J. Tirillò, M. Valente, Post-Impact Mechanical Characterisation of Glass and Basalt Woven Fabric Laminates 2012, Appl Compos Mater, 2012, **19**, 475–490.
13. Emissivity Thermography, *http://www.infrared-thermography.com/material-1.htm,* accessed on December 01, 2015.
14. Schundler, *http://www.schundler.com/polystyrene.htm*, accessed on December 01, 2015.
15. H. Zhao, Q. Xiao, D. Huang, S. Zhang, Influence of Pore Structure on Compressive Strength of Cement Mortar 2014, Scientific World J., **2014**, 1.
16. A.A. Ramezanianour, Cement Replacement Materials (Properties, Durability, Sustainability), Springer-Verlag Berlin Heidelberg, New Delhi, 2014.
17. N.D. Yilmaz, P. Banks-Lee, N.B. Powell, S. Michielsen, Effects of porosity, fiber size, and layering sequence on sound absorption performance of needle-punched nonwovens 2011, J. Appl. Polym. Sci., **121**, 3056.
18. S. Sfarra, C. Ibarra-Castanedo, C. Santulli, D. Paoletti, X. Maldague, Monitoring of jute/hemp fiber hybrid laminates by nondestructive testing techniques, Sci Eng Compos Mater, 2016, **23**, 283, DOI: 10.1515/secm-2013-0138.
19. E. Onofrei, C. Teodor-Cezar, S. Petrusic, G. Bedek, D. Dupont, D. Soulat, Analysis of moisture evaporation from underwear designed for fire-fighters, Autex Research J, 2015, **15**, 35.
20. M. T. Klein, C. Ibarra-Castanedo, A. Bendada, X. Maldague, in Proceedings of the SPIE 6939, Thermosense XXX, 693914, U.S.A., March 2008, edited by V. P. Vavilov & D. D. Burleigh, p. 9.
21. P. Cielo, X. Maldague, A.A. Déom, R. Lewak, Thermographic nondestructive evaluation of industrial materials and structures, Mater Eval, 1987, **45**, 452.
22. J. Allport, J. McHugh, Quantitative evaluation of transient video thermography, Rev Prog Quant Nondestr Eval, 1988, **7A**, 253.
23. X.P.V. Maldague, Theory and practice of infrared technology for nondestructive testing, John Wiley & Sons, Inc., U.S.A., 2001.
24. V.P. Vavilov, R. Taylor, Theoretical and practical aspects of the thermal nondestructive testing of bonded structures, Res Tech Nondestr Test, 1982, **5**, 238.
25. F. Kontoleontos, P. Tsakiridis, A. Marinos, N. Katsiotis, V. Kaloidas, M. Katsioti, Dry-grinded ultrafine cement hydration. Physicochemical and microstructural charaterization, Mater Res, 2013, **16**, 404.
26. J. Fan, L.-li Wang, Q. Cheng, N. Zhu, Y. Liu, Thermal analysis of biomimic woven fabric based on finite element method, J Therm Anal Calorim, 2015, **121**, 737.
27. S. Sfarra, M. Regi, C. Santulli, F. Sarasini, J. Tirillò, S. Perilli, An innovative nondestructive perspective for the prediction of the effect of environmental aging on impacted composite materials, Int J Eng Sci, 2016, **102**, 55, DOI: 10.1016/j.ijengsci.2016.02.009.